Kinematic Optimal Design of a Paramill: A Multi-SP Device

Jun-Ho Lee
Department of Mechanical and Intelligent Systems Engineering
Pusan National University
30 Jangjeon-dong, Geumjeong-gu
Busan, 609-735, Korea
e-mail: junho766@pusan.ac.kr

Keum-Shik Hong*
School of Mechanical Engineering
Pusan National University
30 Jangjeon-dong, Geumjeong-gu
Busan, 609-735, Korea
e-mail: kshong@pusan.ac.kr

Received 20 September 2003; accepted 7 January 2004

In this paper, a manipulability analysis of a new parallel-type rolling mill, named "paramill," in its conceptual design stage is investigated. The paramill considered uses two Stewart platforms (SPs) in opposite directions for the generation of 6 degree-of-freedom motions of individual work-rolls. The objective of this new approach is to pursue an integrated control of the strip thickness, strip shape, pair-crossing angle, uniform wear of the rolls, and tension of the strip. The forward/inverse kinematics problems are formulated. Two main kinematic parameters, the size of the base and the acute angle made by two neighboring joints for a given size of the work-roll, have been determined in the way that the force and moment transmission from the actuators to the work-rolls is maximized. © 2004 Wiley Periodicals, Inc.

1. INTRODUCTION

The continuous rolling is a mechanical process whereby the plastic deformation of a metal (a plate) is achieved by passing it through a series of stands yielding a thin sheet of the metal. Each stand consists of two Stewart platforms (SPs), and each SP has a work-roll and a backup-roll. The role of the backup-roll is to support the work-roll during the rolling.

*To whom all correspondence should be addressed.

Both rolls move up and down together as a unit when the roll gap (strip thickness) is adjusted. Since the middle section of the strip is less deformed than the side edges due to the bendings of the rolls, the upper and lower work-rolls are obliquely placed. The oblique placement of the two work-rolls is called a pair-crossing, with which a uniform thickness across the strip is achieved. To adjust the pair-crossing angle of the rolls, two additional hydraulic cylinders are used. In the conventional mill, the degrees of freedom (DOF) of a roll is 3: heave (up and down motion), pair-crossing (yawing), and rolling.

In the current rolling mill, once the roll gap and the pair-crossing angle are set up, they cannot be modified during the process. Only the roll velocity and the looper angle for adjusting the strip tension can be adjusted. Therefore, an integrated (simultaneous) control of the strip thickness, strip tension, strip shape, and uniform wear of the roll is not possible. This necessitates the development of a new rolling technology, which can provide sufficient degrees of freedom to the work-rolls (at least five degrees of freedom). The proposed paramill is based upon a SP type manipulator.[1,2] Its manipulability analysis has already been addressed in Reference 3. However, the work in Reference 3 has considered only one SP, not two SPs in opposite directions, which would represent the actual rolling process better.

The rolling process needs high power consumption and an accurate control. For a SP type manipulator, six hydraulic actuators are located in parallel, so that the rolling force can be evenly distributed. Also, in comparison with a serial manipulator, the positioning accuracy of the end-effector (the work-roll) is better, the structural stiffness is higher, and the dynamic response time is superior, too. On the other hand, the workspace of a parallel manipulator is relatively small. Such a small workspace is an evident weakness in general; however, this would not be a shortcoming for a paramill, because the workspace for rolling is quite small. Each SP considered in this paper consists of a platform, a base, and six hydraulic legs. Hence, by attaching a work-roll to the platform, 6 DOF motions of the roll can be made.

In this paper, a conceptual design of the paramill is presented in the way that power transmission from the actuators to the end-effector is maximized. The authors do not claim that the paramill should be designed in this fashion only, but would rather suggest one way of designing. Note that an integrated control needs at least 5 DOF motions of the work-roll: surge (strip tension control), sway (even wear across the roll), heave (strip thickness control), rolling (strip shape control), and yawing (even thickness across the strip). Even though the SP[1] can provide 6 DOF motions, the pitch motion of the roll is not considered because the roll itself is rotating. The paramill then will make the looper mechanism obsolete, which is the current technology for tension control.

The design problem considered in this paper discusses the determination of a stand size for a given size of the work-roll. Therefore, the size of the base, configuration of the joints, and lengths of hydraulic cylinders have to be decided. The results of Hong et al.[3] that considered only one SP in the kinematic design would not be sufficient because the analysis by Hong et al.[3] did not consider the rolling force and moment generated between the two work-rolls in contact.

The forward kinematics problem is defined as the problem of finding the roll-gap and the pair-crossing angle of the two work-rolls for given lengths of 12 legs, six from each SP. On the other hand, the inverse kinematics problem is defined as the problem of finding the lengths of 12 legs when the roll-gap, the pair-crossing angle, and the position and orientation of one work-roll are given. A kinematic constraint equation, in the configuration where two SPs are in contact at its neutral position, is first derived. From the kinematic constraint equation, a velocity–Jacobian matrix and a subsequent force–Jacobian matrix are derived. A manipulability measure, which is a ratio of the manipulability ellipsoid volume and the condition number of each velocity/force-Jacobian matrix, is defined. Two main kinematic parameters, the size of the base and the acute (opening) angle of two neighboring joints, have been determined in the way that the force and moment transmissions from the actuators to the work-roll are maximized. The results will be compared with the results of ref. 3.

This paper is organized as follows: Section 2 describes the rolling process briefly and introduces the coordinate systems of the paramill. In Section 3, kinematic constraint equations are derived and then the forward and inverse kinematics problems are analyzed. In Section 4, Jacobian matrices are derived and the workspace is discussed. In Section 5, the manipulability analysis of the paramill in terms of link lengths and joint angles is performed and the optimal link lengths are proposed. Finally, Section 6 concludes the paper.

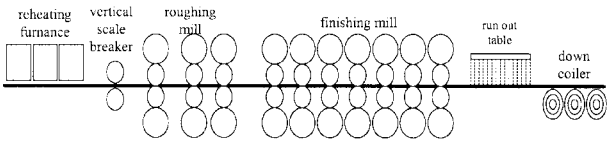

Figure 1. A schematic of the current continuous rolling mill facility.

2. PRELIMINARIES: ROLLING PROCESS AND PARAMILL STRUCTURE

2.1. Rolling Process

Rolling is the process of forming metal (steel, aluminum, etc.) sheets from slab ingots. The slab is normally preheated in a furnace and rolled between powered rollers. The main difference between hot and cold rollings is that in hot rolling the workpiece is initially at, or is heated to, above recrystallization temperature, as contrasted to cold rolling, where the workpiece is processed at ambient temperature.[4]

Figure 1 shows a schematic of the current continuous rolling mill facility. The process route can best be described in terms of the major items of equipment as follows:[5] The feed stock for the rolling mill are slabs produced by the continuous casting process in a steel plant. Therefore, the slabs at ambient temperature are first sent to a reheat furnace to raise the temperature of the whole slab to around 1300 °C. On exit from the reheat furnace, there is a buildup of scale on the surface of the slab, due to oxidation, which is detrimental to the surface quality. This is removed within the descaling box, which consists of jets of high-pressure water. And then the slab is sent to a roughing mill, which is a reversing mill that produces a breakdown bar by rolling the slab through a series of forward and reverse passes, typically reducing the slab thickness from 200 to 30 mm. After removing any variations in the leading edge of the breakdown bar and descaling, the slab is finally sent to a finishing mill, which is designed to reduce the thickness of the breakdown bar to that of the finished coil, while maintaining the desired width. A sequential combination of stands, from two to six, is used depending on the product being rolled. The mill control system is critical, because a constant mass flow must be maintained in all stands to ensure continuous production.

On exit from the finishing mill, the product, which is typically above 800 °C, is cooled at a run-out table. On exit from the mill/run-out table cooling system, the hot product typically has a velocity of up to 40 m per hour and can be hundreds of meters in length. The down coiler finally allows the product to be converted into a coil of dimensions that can be easily transported.

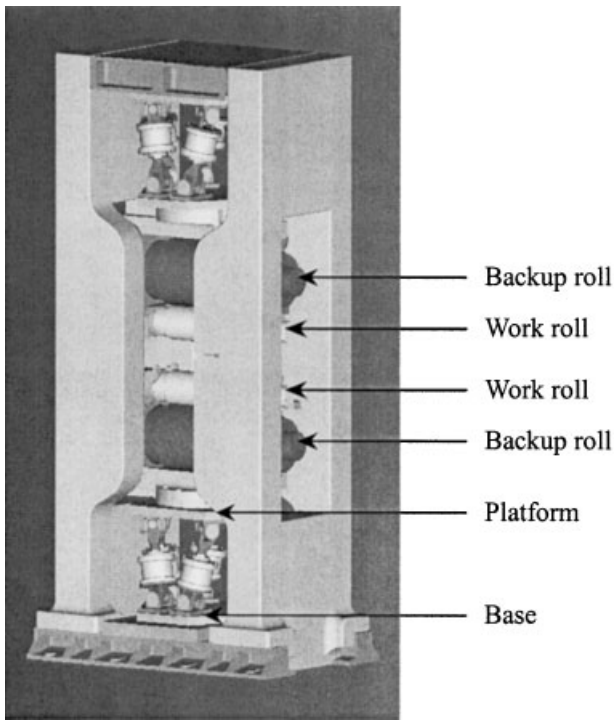

Figure 2. A 3D graphics of the paramill based upon two Stewart platforms.

2.2. Paramill Configuration

Figure 2 shows a 3D graphic of the paramill based upon two SPs. Figure 3 depicts a schematic of the

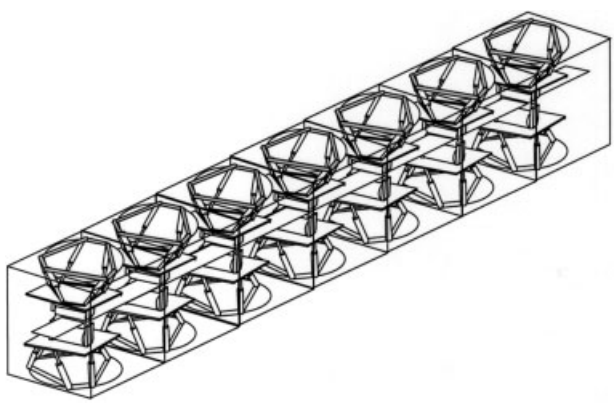

Figure 3. The proposed continuous rolling process that uses seven paramills.

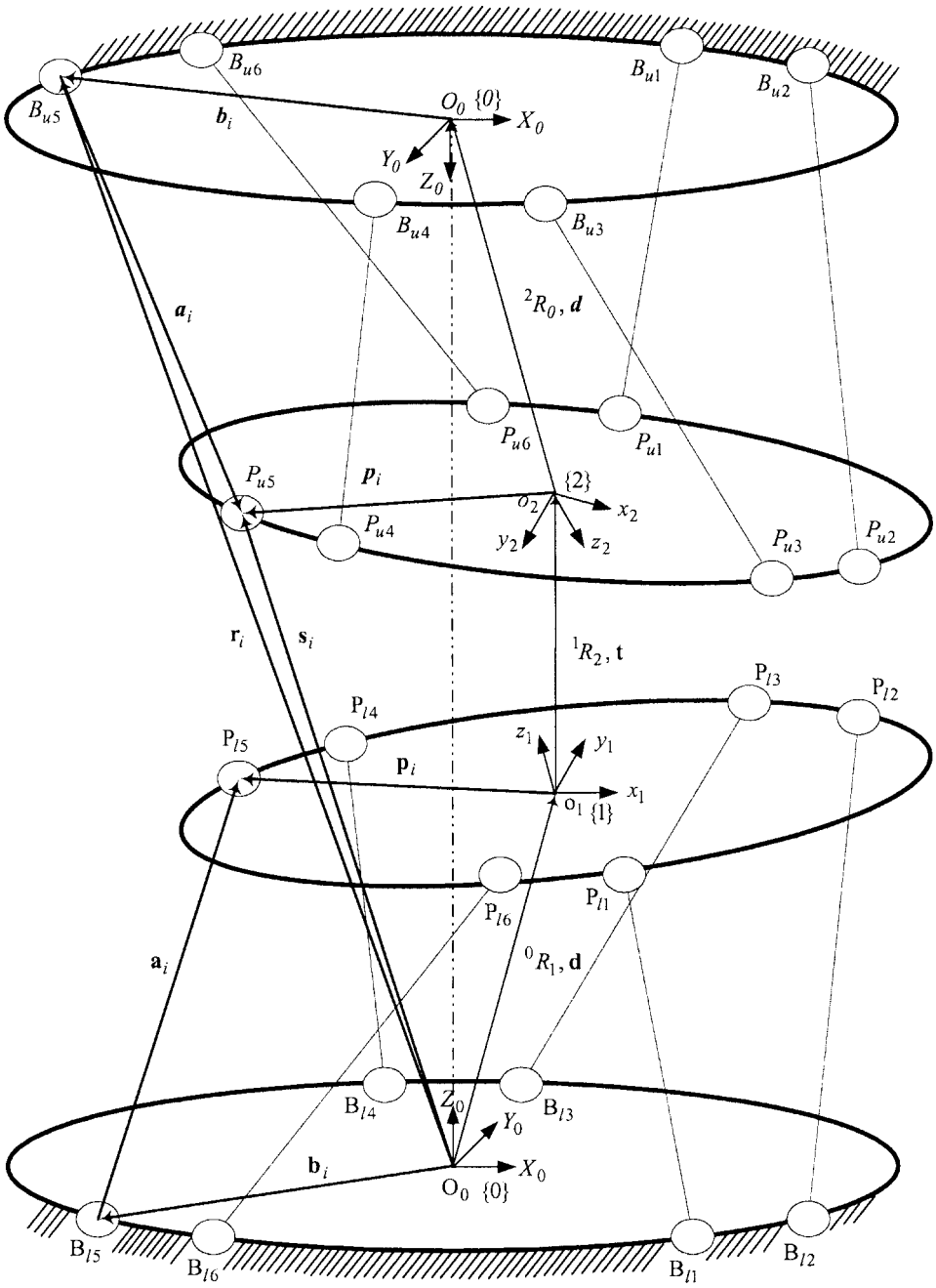

Figure 4. The coordinate systems introduced for the paramill.

proposed continuous rolling process, which uses seven paramills. Figure 4 shows the coordinate systems introduced for the paramill, which are attached to the bases and platforms.

The coordinate systems for the lower SP are first introduced: Let {0} be the coordinate system that is attached to the base, which is a fixed coordinate system denoting $X_0-Y_0-Z_0$ directions. The origin of {0} is O_0, which is the center of the base. Let {1} be the coordinate system that is attached to the platform, which is a moving coordinate system denoting $x_1-y_1-z_1$ directions. The origin of {1} is o_1, which is the center of the platform. Let B_i and P_i ($i=1,2,\ldots,6$) denote six joints on the base and on the platform, respectively. Let $\mathbf{b}_i=\overline{O_0B_i}$ and $\mathbf{p}_i=\overline{o_1P_i}$

($i=1,2,...,6$) be the position vectors from the origins of the base and platform to the corresponding joints, respectively. Let $\mathbf{a}_i=\overline{B_iP_i}$ ($i=1,2,...,6$) be the leg vectors from the six joints on the base to the six joints on the platform. Let ${}^0R_1$ and $\mathbf{d}=\overline{O_0o_1}=[d_X\ \ d_Y\ \ d_Z]^T$ be the rotation matrix and translation vector between {0} and {1}, respectively.

A similar notation can be introduced for the upper SP. Note that all variables for the upper SP are written in italic, while those for the lower SP are written in normal face. Let {*0*} the coordinate system attached to the base of the upper SP, which is a fixed coordinate system denoting $X_0-Y_0-Z_0$ directions. Note that {*0*} has been rotated by $R_{X_0}(\pi)$ with respect to {*0*}, i.e., 180 degrees with respect to the X_0-axis of the lower SP. Let O_0 denote the center of the base of the upper SP. Let {2} denote the coordinate system attached to the platform of the upper SP. {2} is a moving coordinate system denoting $x_2-y_2-z_2$ directions, whose origin is o_2. Let B_i and P_i ($i=1,2,...,6$) denote the six joints on the base and platform in the upper SP, respectively. Let $p_i=\overline{o_2P_i}$ and $b_i=\overline{O_0B_i}$ ($i=1,2,...,6$) be the position vectors to the joints. The leg vectors of the upper SP are $a_i=\overline{B_iP_i}$ ($i=1,2,...,6$). Let ${}^2R_0$ and $d=\overline{o_2O_0}=[d_x\ \ d_y\ \ d_z]^T$ be the rotation matrix and translation vector from the moving coordinate {2} to the fixed coordinate {*0*}.

Since the motions of two SPs are not independent, two auxiliary vectors $\mathbf{r}_i=\overline{O_0B_i}$ and $\mathbf{s}_i=\overline{O_0P_i}$ ($i=1,2,...,6$) are introduced as intermediate variables for clarifying the dependence; see Figure 4. Let ${}^O\mathbf{d}_O=\overline{O_0O_0}$ be the vector from the origin of {0}-coordinate to that of {*0*}-coordinate. Let ${}^1R_2$ and $\mathbf{t}=[t_x\ \ t_y\ \ t_z]^T$ be the rotation matrix and translational vector from {1}-coordinate to {2}-coordinate, respectively, where $\mathbf{t}$ denotes the thickness of the strip.

Let the rotation matrix of the platform of the lower SP with respect to {0}-coordinate be ${}^0R_1=R_{Z_0}(\gamma)R_{Y_0}(\beta)R_{X_0}(\alpha)$, where α,β,γ denote the fixed angle representation. Similarly, let the rotation matrix of the platform of the upper SP with respect to {*0*}-coordinate be ${}^0R_2=({}^2R_0)^{-1}=R_{Z_0}(\gamma')R_{Y_0}(\beta')R_{X_0}(\alpha')$, where α',β',γ' denote the fixed angle representation for the upper SP. Note that α, β, γ and α',β',γ' represent the rolling, pitching, and yawing angles of the individual platforms. Hence, ${}^1R_2$ can be determined from ${}^0R_1$ and ${}^0R_2$.

Finally, Figure 5 shows the configuration of the joints on the base and platform for connecting the hydraulic cylinders. Such an arrangement in Figure 5 can avoid a kinematic singularity.[6–9] It is noted that the center lines (solid) bisecting two neighboring joints make 120 degree obtuse angles. Let the acute angle made by the center line and one neighboring joint on the base and platform be ϕ_{lb} and ϕ_{lp} for the lower SP, respectively, and ϕ_{ub} and ϕ_{up} for the upper SP, respectively.

Design Objective: In this paper, the two design parameters pursued are the radius of the base, r_{lb}, and the acute angle, ϕ_{lb}, for a given radius of the platform. For the paramill, seven parameters, i.e., r_{lb}, r_{ub}, ϕ_{lb}, ϕ_{lp}, ϕ_{ub}, ϕ_{up}, and ${}^O\mathbf{d}_O=\overline{O_0O_0}$, would affect a manipulability of the paramill. But, because a symmetric structure of the paramill is desired and the complexity of the optimization problem should be in a manageable form, $r_{lb}=r_{ub}$ and $\phi_{lb}=\phi_{lp}=\phi_{ub}=\phi_{up}$ are assumed. Also, ${}^O\mathbf{d}_O$ is assumed a given value. Therefore, through the analyses in Sections 3 and 4 next, the base radius $r_{lb}(=r_{ub})$ and the acute angle $\phi_{lb}(=\phi_{lp}=\phi_{ub}=\phi_{up})$ are optimally designed.

3. KINEMATIC ANALYSIS OF PARAMILL

3.1. Kinematic Constraints

Since a paramill involves two SPs, the motion of the upper work-roll is not independent from the motion of the lower one. The contact motion with a given roll gap has to be maintained at all times, yielding a closed-loop chain. Therefore, the kinematics problem should be looked into as a constraint problem of a closed kinematic chain.

First, in Figure 4, the leg vectors $\mathbf{a}_i$ of the lower SP are derived as

$$\mathbf{a}_i=\mathbf{d}-\mathbf{b}_i+{}^0R_1\,{}^1\mathbf{p}_i,\quad i=1,2,...,6, \tag{1}$$

where the superscript in the left-hand side of ${}^1\mathbf{p}$ denotes the {1} coordinate system. In such a situation where a misunderstanding might occur, the left-hand superscript like 0 in ${}^0R_1$ or 1 in ${}^1\mathbf{p}$ will be added. However, if the used coordinate system is quite clear, it will be skipped. The $\mathbf{r}_i$ and $\mathbf{s}_i$ vectors in Figure 4 are

$$\mathbf{r}_i=\mathbf{d}+{}^0R_1\,{}^1\mathbf{t}+{}^0R_2\,{}^2\boldsymbol{d}+{}^0R_0\boldsymbol{b}_i,\quad i=1,2,...,6, \tag{2}$$

$$\mathbf{s}_i=\mathbf{d}+{}^0R_1\,{}^1\mathbf{t}+{}^0R_2\,{}^2\boldsymbol{p}_i,\quad i=1,2,...,6. \tag{3}$$

Hence, the leg vectors $\boldsymbol{a}_i$ of the upper SP become

$$\boldsymbol{a}_i=-\mathbf{r}_i+\mathbf{s}_i,\quad i=1,2,...,6. \tag{4}$$

The substitution of (2) and (3) into (4) yields

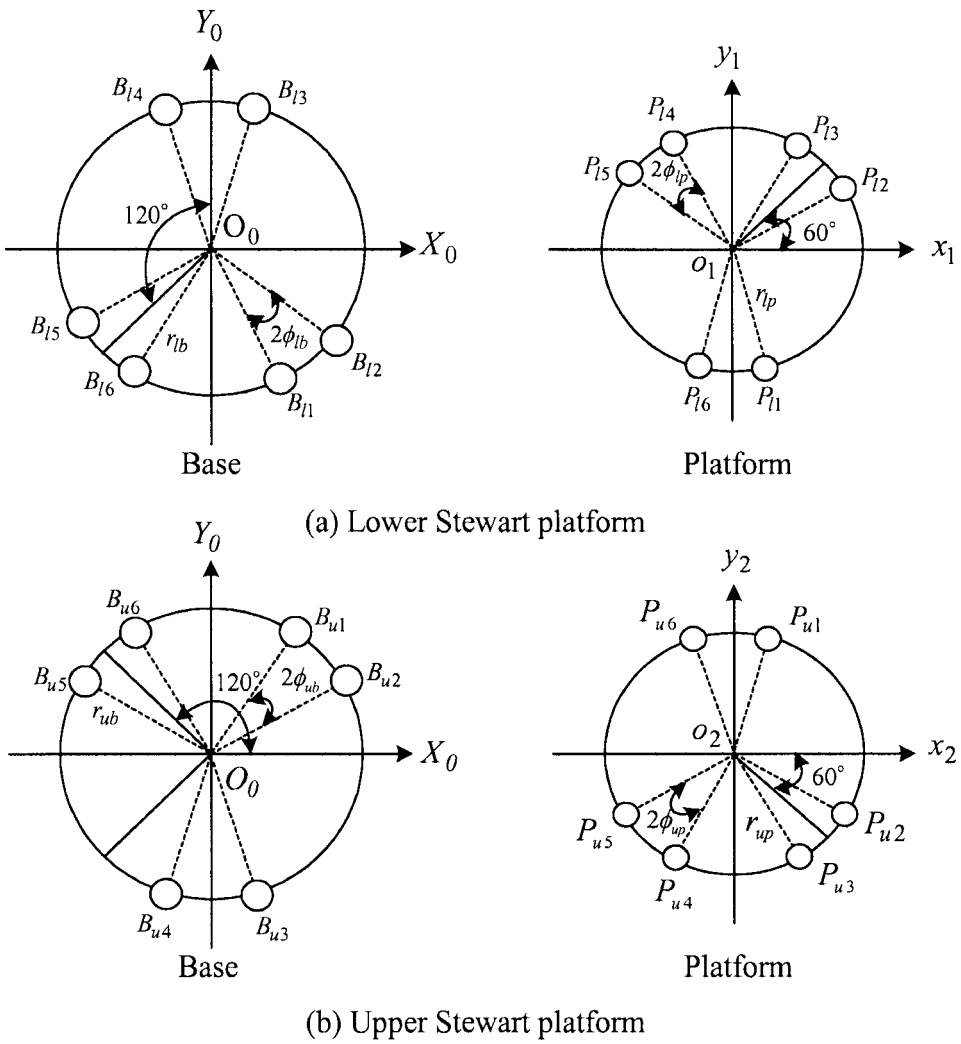

Figure 5. The joints configuration for connecting hydraulic cylinders.

$$\boldsymbol{a}_i = -(\mathbf{d} + {}^0R_1\,{}^1\mathbf{t} + {}^0R_2\,{}^2\boldsymbol{d} + {}^0R_0\boldsymbol{b}_i) + \mathbf{d} + {}^0R_1\,{}^1\mathbf{t} + {}^0R_2\,{}^2\boldsymbol{p}_i$$
$$= {}^0R_2(-{}^2\boldsymbol{d} - {}^2R_0\boldsymbol{b}_i + {}^2\boldsymbol{p}_i), \quad i = 1,2,\ldots,6. \tag{5}$$

The multiplication of $({}^0R_2)^{-1}$ at both sides of (5) yields

$$({}^0R_2)^{-1}\boldsymbol{a}_i = -{}^2\boldsymbol{d} - {}^2R_0\boldsymbol{b}_i + {}^2\boldsymbol{p}_i, \quad i = 1,2,\ldots,6. \tag{6}$$

The re-arrangement of the terms in (6) yields

$${}^2\boldsymbol{d} = -{}^2R_0\boldsymbol{b}_i + {}^2\boldsymbol{p}_i - ({}^0R_2)^{-1}\boldsymbol{a}_i, \quad i = 1,2,\ldots,6. \tag{7}$$

The distance from O_0 to O_0 is

$${}^0\mathbf{d}_0 = \mathbf{d} + {}^0R_1\,{}^1\mathbf{t} + {}^0R_2\,{}^2\boldsymbol{d}. \tag{8}$$

Finally, by substituting (1) and (7) into (8), the constraint equation is derived as follows:

$${}^0\mathbf{d}_0 = \mathbf{a}_i + \mathbf{b}_i - {}^0R_1\,{}^1\mathbf{p}_i\,{}^0R_1\,{}^1\mathbf{t} - {}^0R_0\boldsymbol{b}_i + {}^0R_2\,{}^2\boldsymbol{p}_i - \boldsymbol{a}_i,$$
$$i = 1,2,\ldots,6, \tag{9}$$

where ${}^0\mathbf{d}_0$ denotes the constant vector given by the height of a stand. Hence, $\boldsymbol{a}_i$ becomes

$$\boldsymbol{a}_i = \mathbf{a}_i + \mathbf{b}_i - {}^0R_1\,{}^1\mathbf{p}_i + {}^0R_1\,{}^1\mathbf{t} - {}^0R_0\boldsymbol{b}_i + {}^0R_2\,{}^2\boldsymbol{p}_i - {}^0\mathbf{d}_0,$$
$$i = 1,2,\ldots,6. \tag{10}$$

3.2. Inverse Kinematics

The inverse kinematics problem of the paramill is defined as the problem of finding the 12 leg lengths of

the two SPs for a given roll-gap and pair-crossing angle. This problem becomes equivalent to the problem of finding the lengths of six legs of individual SPs once the orientation and position of one work-roll is further given. This is because once the roll gap, the pair-crossing angle, and the position and orientation of one roll are determined, the position and orientation of another roll are automatically determined. In this case, $\mathbf{a}_i$ $(i=1,2,...,6)$ can be pursued for given $\mathbf{d}$ and ${}^0R_1$ and $\boldsymbol{a}_i$ $(i=1,2,...,6$ can be pursued for given $\boldsymbol{d}$ and ${}^2R_0$.

Now, assume that $\mathbf{d}$, ${}^0R_1$, $\mathbf{t}$ (roll gap), and ${}^1R_2$ (pair-crossing angle) are given. Therefore, the leg lengths in the lower SP from (1) are given as

$$\|\mathbf{a}_i\|^2=(\mathbf{d}-\mathbf{b}_i+{}^0R_1\,{}^1\mathbf{p}_i)\cdot(\mathbf{d}-\mathbf{b}_i+{}^0R_1\,{}^1\mathbf{p}_i)$$

$$(i=1,2,...,6), \tag{11}$$

where $\mathbf{b}_i=[r_{lb}\cos\theta_{lbi}\ \ r_{lb}\sin\theta_{lbi}\ \ 0]^T$, ${}^1\mathbf{p}_i=[r_{lp}\cos\theta_{lpi}\ \ r_{lp}\sin\theta_{lpi}\ \ 0]^T$, $(i=1,2,...,6)$. Similarly, the substitution of (1) into (10) yields

$$\boldsymbol{a}_i={}^0R_1\,{}^1R_2\,{}^2\boldsymbol{p}_i-{}^0R_1\,{}^1R_2\,{}^2R_0\,{}^0\boldsymbol{b}_i+{}^0R_1\,{}^1\mathbf{t}+\mathbf{d}-{}^0\mathbf{d}_0, \tag{12}$$

where $\boldsymbol{b}_i=[r_{ub}\cos\eta_{ubi}\ \ r_{ub}\sin\eta_{ubi}\ \ 0]^T$, $\boldsymbol{p}_i=[r_{up}\cos\eta_{upi}\ \ r_{up}\sin\eta_{upi}\ \ 0]^T$ $(i=1,2,...,6)$. Hence, the leg lengths in the upper SP are

$$\begin{aligned}\|\boldsymbol{a}_i\|^2=&({}^0R_1\,{}^1R_2\,{}^2\boldsymbol{p}_i-{}^0R_1\,{}^1R_2\,{}^2R_0\,{}^0\boldsymbol{b}_i+{}^0R_1\,{}^1\mathbf{t}+\mathbf{d}-{}^0\mathbf{d}_0)\\&\cdot({}^0R_1\,{}^1R_2\,{}^2\boldsymbol{p}_i-{}^0R_1\,{}^1R_2\,{}^2R_0\,{}^0\boldsymbol{b}_i+{}^0R_1\,{}^1\mathbf{t}+\mathbf{d}\\&-{}^0\mathbf{d}_0),\quad i=1,2,...,6.\end{aligned} \tag{13}$$

Note that $\|\mathbf{a}_i\|$ are given in terms of $\mathbf{d}$ and ${}^0R_1$ and $\|\boldsymbol{a}_i\|$ are given with additional $\mathbf{t}$ and ${}^1R_2$.

3.3. Direct Kinematics Analysis

For a single SP, the forward kinematics problem is defined as the problem of finding the position and orientation of the platform for given lengths of the six legs. For a parallel manipulator, the forward kinematics solutions are known to be nonunique and therefore a numerical approach or the use of extra sensors is sometimes pursued.[10,11]

For the paramill, the forward kinematics problem is defined as the problem of finding the roll gap and pair-crossing angle via the position and orientation information of individual work-rolls for given lengths of the two SPs. Hence, following the works in the literature,[2] $\mathbf{d}$ and ${}^0R_1$ can be pursued for given leg lengths of the lower SP and similarly $-\boldsymbol{d}$ and ${}^0R_2$ can be pursued for given leg lengths of the upper SP.

Since the {0} coordinate system of the upper SP has rotated 180 degrees with respect to the X_0-axis in the lower SP, the rotation matrix between the two frames, ${}^0R_0$, has the relationship ${}^0R_0={}^2R_0\,{}^1R_2\,{}^0R_1$ and therefore the rotation matrix between the two work-rolls becomes

$${}^1R_2=({}^2R_0)^{-1}\,{}^0R_0({}^0R_1)^{-1}. \tag{14}$$

Also, once $\mathbf{d}$, ${}^0R_1$, $\boldsymbol{d}$, ${}^0R_2$ are determined for given lengths of the 12 legs, the roll gap $\mathbf{t}$ is obtained using (10) and (14) as follows:

$$\begin{aligned}\mathbf{t}=&({}^0R_1)^{-1}(\boldsymbol{a}_i-\mathbf{a}_i-\mathbf{b}_i+{}^0d_0)+{}^1\mathbf{p}_i\\&+(({}^2R_0)^{-1}\,{}^0R_0({}^0R_1)^{-1})({}^2R_0\boldsymbol{b}_i)\\&-(({}^2R_0)^{-1}\,{}^0R_0({}^0R_1)^{-1})({}^2\boldsymbol{p}_i),\quad i=1,2,...,6.\end{aligned} \tag{15}$$

Therefore, as forward kinematics solutions of Paramill, the relative orientation of two work-rolls is given in (14) and their relative position in (15), respectively.

4. JACOBIAN MATRICES AND WORK SPACE

In this section, the velocity and force Jacobian matrices of the paramill are derived and the associated workspace is discussed. For a single SP, the velocity Jacobian matrix is the transformation that allows the calculation of the linear and angular velocities of the platform for given linear velocities of the legs. Also, the force/moment Jacobian matrices is the transformation that converts the axial forces at the six legs to the resultant force and moment of the platform, respectively.[12,3]

The velocity Jacobian matrix proposed for the paramill is the transformation that maps the linear velocities at the 12 legs to the relative velocity and relative angular velocity between the two work-rolls. Also, the force and moment Jacobian matrix, which is derived from the velocity Jacobian matrix using the principle of virtual work, allows the calculation of the resultant rolling force and moment at the two work-rolls for given actuating forces at the 12 legs.

4.1. Velocity Jacobian Matrix

Using the constraint equations (1) and (10), the velocity Jacobian matrix is derived as follows: First, the inner product of (1) yields

$$\mathbf{a}_i \cdot \mathbf{a}_i = \mathbf{a}_i \cdot (\mathbf{d} - \mathbf{b}_i + {}^0R_1\,{}^1\mathbf{p}_i), \quad i = 1,2,\ldots,6. \tag{16}$$

Differentiating (16) with respect to time and using $(d/dt)({}^0R_1) = \boldsymbol{\omega}_l \times {}^0R_1$,[13] the following expression is derived:

$$\begin{aligned}\mathbf{a}_i \cdot \dot{\mathbf{a}}_i &= \mathbf{a}_i \cdot (\dot{\mathbf{d}} + \boldsymbol{\omega}_l \times {}^0R_1\,{}^1\mathbf{p}_i)\\ &= \mathbf{a}_i \cdot \dot{\mathbf{d}} + \mathbf{a}_i \cdot (\boldsymbol{\omega}_l \times {}^0R_1\,{}^1\mathbf{p}_i)\\ &= \mathbf{a}_i \cdot \dot{\mathbf{d}} + {}^0R_1\,{}^1\mathbf{p}_i \cdot (\mathbf{a}_i \times \boldsymbol{\omega}_l)\\ &= \mathbf{a}_i \cdot \dot{\mathbf{d}} + \boldsymbol{\omega}_l \cdot {}^0R_1\,{}^1\mathbf{p}_i \times \mathbf{a}_i, \quad i = 1,2,\ldots,6,\end{aligned} \tag{17}$$

where $\boldsymbol{\omega}_l = [\omega_{l_X}\ \ \omega_{l_Y}\ \ \omega_{l_Z}]^T$ denotes the angular velocity vector of the lower platform. Also, the inner product of (10) yields

$$\begin{aligned}\boldsymbol{a}_i \cdot \boldsymbol{a}_i &= \boldsymbol{a}_i \cdot (\mathbf{a}_i + \mathbf{b}_i - {}^0R_1\,{}^1\mathbf{p}_i + {}^0R_1\,{}^1\mathbf{t} - {}^0R_0\boldsymbol{b}_i\\ &\quad + {}^0R_2\,{}^2\boldsymbol{p}_i - {}^0\mathbf{d}_0)\\ &= \boldsymbol{a}_i \cdot (\mathbf{a}_i + \mathbf{b}_i - {}^0R_1\,{}^1\mathbf{p}_i + {}^0R_1\,{}^1\mathbf{t} - {}^0R_1\,{}^1R_2\,{}^2R_0\boldsymbol{b}_i\\ &\quad + {}^0R_1\,{}^1R_2\,{}^2\boldsymbol{p}_i - {}^0\mathbf{d}_0),\\ &\quad i = 1,2,\ldots,6.\end{aligned} \tag{18}$$

The differentiation of (18) with respect to time yields

$$\begin{aligned}\boldsymbol{a}_i \cdot \dot{\boldsymbol{a}}_i &= \boldsymbol{a}_i \cdot [\dot{\mathbf{a}}_i + \dot{\mathbf{b}}_i - ({}^0\dot{R}_1\,{}^1\mathbf{p}_i + {}^0R_1\,{}^1\dot{\mathbf{p}}_i) + ({}^0\dot{R}_1\,{}^1\mathbf{t}\\ &\quad + {}^0R_1\,{}^1\dot{\mathbf{t}}) - ({}^0\dot{R}_1\,{}^1R_2\,{}^2R_0\mathbf{b}_i + {}^0R_1\,{}^1\dot{R}_2\,{}^2R_0\boldsymbol{b}_i\\ &\quad + {}^0R_1\,{}^1R_2\,{}^2\dot{R}_0\boldsymbol{b}_i + {}^0R_1\,{}^1R_2\,{}^2R_0\dot{\boldsymbol{b}}_i) + ({}^0\dot{R}_1\,{}^1R_2\,{}^2\boldsymbol{p}_i\\ &\quad + {}^0R_1\,{}^1\dot{R}_2\,{}^2\boldsymbol{p}_i + {}^0R_1\,{}^1R_2\,{}^2\dot{\boldsymbol{p}}_i) - {}^0\dot{\mathbf{d}}_0], \quad i = 1,2,\ldots,6.\end{aligned} \tag{19}$$

Since ${}^0\mathbf{d}_0, \boldsymbol{p}_i, \boldsymbol{b}_i, \mathbf{p}_i, \mathbf{b}_i$ are constant vectors, ${}^0\dot{\mathbf{d}}_0 = \dot{\boldsymbol{p}}_i = \dot{\boldsymbol{b}}_i = \dot{\mathbf{p}}_i = \dot{\mathbf{b}}_i = 0$ holds. Rearranging the terms in (19) yields

$$\begin{aligned}\boldsymbol{a}_i \cdot \dot{\boldsymbol{a}}_i &= \boldsymbol{a}_i \cdot [\dot{\mathbf{a}}_i - ({}^0\dot{R}_1\,{}^1\mathbf{p}_i) + ({}^0\dot{R}_1\,{}^1\mathbf{t} + {}^0R_1\,{}^1\dot{\mathbf{t}})\\ &\quad - ({}^0\dot{R}_1\,{}^1R_2\,{}^2R_0\boldsymbol{b}_i + {}^0R_1\,{}^1\dot{R}_2\,{}^2R_0\boldsymbol{b}_i\\ &\quad + {}^0R_1\,{}^1R_2\,{}^2\dot{R}_0\boldsymbol{b}_i) + ({}^0\dot{R}_1\,{}^1R_2\,{}^2\boldsymbol{p}_i\\ &\quad + {}^0R_1\,{}^1\dot{R}_2\,{}^2\boldsymbol{p}_i], \quad i = 1,2,\ldots,6.\end{aligned} \tag{20}$$

Using $(d/dt)({}^1R_2) = \boldsymbol{\omega}_{pc} \times {}^1R_2$ and $(d/dt)({}^2R_0) = \boldsymbol{\omega}_u \times {}^2R_0$ where the subscript pc stands for the pair-crossing, the following expression is derived:

$$\begin{aligned}\boldsymbol{a}_i \cdot \dot{\boldsymbol{a}}_i &= \boldsymbol{a}_i \cdot [\dot{\mathbf{a}}_i - (\boldsymbol{\omega}_l \times {}^0R_1\,{}^1\mathbf{p}_i) + (\boldsymbol{\omega}_l \times {}^0R_1\,{}^1\mathbf{t} + {}^0R_1\,{}^1\dot{\mathbf{t}})\\ &\quad - (\boldsymbol{\omega}_l \times {}^0R_1\,{}^1R_2\,{}^2R_0\boldsymbol{b}_i + {}^0R_1\boldsymbol{\omega}_{pc} \times {}^1R_2\,{}^2R_0\boldsymbol{b}_i\\ &\quad + {}^0R_1\,{}^1R_2\boldsymbol{\omega}_u \times {}^2R_0\boldsymbol{b}_i) + (\boldsymbol{\omega}_l \times {}^0R_1\,{}^1R_2\,{}^2\boldsymbol{p}_i\\ &\quad + {}^0R_1\boldsymbol{\omega}_{pc} \times {}^1R_2\,{}^2\boldsymbol{p}_i], \quad i = 1,2,\ldots,6,\end{aligned} \tag{21}$$

where $\boldsymbol{\omega}_u = [\omega_{uX}\ \ \omega_{uY}\ \ \omega_{uZ}]^T$ is the angular velocity vector of the upper platform, $\boldsymbol{\omega}_{pc} = [\omega_{pcx}\ \ \omega_{pcy}\ \ \omega_{pcz}]^T$ is the relative angular velocity vector of the two work-rolls. $\boldsymbol{\omega}_l$, $\boldsymbol{\omega}_u$, and $\boldsymbol{\omega}_{pc}$ satisfy the following relationship (22), because the vector from O_0 to O_0 is a constant vector with no rotational motion:

$$\begin{aligned}&\boldsymbol{\omega}_l + {}^0R_1\boldsymbol{\omega}_{pc} + {}^0R_1\,{}^1R_2\boldsymbol{\omega}_u = \mathbf{0},\\ &{}^0R_1\,{}^1R_2\boldsymbol{\omega}_u = -\boldsymbol{\omega}_l - {}^0R_1\boldsymbol{\omega}_{pc}.\end{aligned} \tag{22}$$

The substitution of $\dot{\mathbf{a}}_i = \dot{\mathbf{d}} + \boldsymbol{\omega}_l \times {}^0R_1\,{}^1\mathbf{p}_i$ and (22) into (21) yields

$$\begin{aligned}\boldsymbol{a}_i \cdot \dot{\boldsymbol{a}}_i &= \boldsymbol{a}_i \cdot \dot{\mathbf{d}} + \boldsymbol{a}_i \cdot (\boldsymbol{\omega}_l \times ({}^0R_1\,{}^1\mathbf{t} - {}^0R_1\,{}^1R_2\,{}^2R_0\boldsymbol{b}_i + {}^2R_0\boldsymbol{b}_i\\ &\quad + {}^0R_1\,{}^1R_2\,{}^2\boldsymbol{p}_i)) + \boldsymbol{a}_i \cdot (-{}^0R_1\boldsymbol{\omega}_{pc} \times ({}^1R_2\,{}^2R_0\boldsymbol{b}_i\\ &\quad - {}^2R_0\boldsymbol{b}_i - {}^1R_2\,{}^2\boldsymbol{p}_i)) + \boldsymbol{a}_i \cdot ({}^0R_1\,{}^1\dot{\mathbf{t}})\\ &= \boldsymbol{a}_i \cdot \dot{\mathbf{d}} + \boldsymbol{\omega}_l \cdot ({}^0R_1\,{}^1\mathbf{t} - {}^0R_1\,{}^1R_2\,{}^2R_0\boldsymbol{b}_i\\ &\quad + {}^2R_0\boldsymbol{b}_i + {}^0R_1\,{}^1R_2\,{}^2\boldsymbol{p}_i) \times \boldsymbol{a}_i - {}^0R_1\boldsymbol{\omega}_{pc} \cdot ({}^1R_2\,{}^2R_0\boldsymbol{b}_i\\ &\quad - {}^2R_0\boldsymbol{b}_i - {}^1R_2\,{}^2\boldsymbol{p}_i) \times \boldsymbol{a}_i + \boldsymbol{a}_i \cdot ({}^0R_1\,{}^1\dot{\mathbf{t}}),\\ &\quad i = 1,2,\ldots,6.\end{aligned} \tag{23}$$

A matrix representation of (17) and (23) becomes

$$L\dot{\mathbf{l}} = M\dot{\mathbf{o}},$$

where

$$\dot{\mathbf{l}}=[\|\dot{a}_1\|\cdots\|\dot{a}_6\|\|\dot{a}_1\|\cdots\|\dot{a}_6\|]^T,$$

$$\dot{\mathbf{o}}=[\dot{d}_X \quad \dot{d}_Y \quad d_Z \quad \omega_{lX} \quad \omega_{lY} \quad \omega_{lZ} \quad \dot{t}_x \quad \dot{t}_y \quad \dot{t}_z \quad \omega_{pcx} \quad \omega_{pcy} \quad \omega_{pcz}]^T,$$

$$L=\begin{bmatrix} \|a_1\| & & & & & \\ & \ddots & & & \mathbf{0}_{6\times 6} & \\ & & \|a_6\| & & & \\ & & & \|a_1\| & & \\ & \mathbf{0}_{6\times 6} & & & \ddots & \\ & & & & & \|a_6\| \end{bmatrix},$$

$$M=\begin{bmatrix} \mathbf{a}_1^T & (A_1\times\mathbf{a}_1)^T & \mathbf{0}_{1\times 3} & \mathbf{0}_{1\times 3} \\ \vdots & \vdots & \vdots & \vdots \\ \mathbf{a}_6^T & (A_6\times\mathbf{a}_6)^T & \mathbf{0}_{1\times 3} & \mathbf{0}_{1\times 3} \\ \boldsymbol{a}_1^T & (B_1\times\boldsymbol{a}_1)^T & -{}^0R_1\boldsymbol{a}_1^T & (C_1\times\boldsymbol{a}_1)^T \\ \vdots & \vdots & \vdots & \vdots \\ \boldsymbol{a}_6^T & (B_6\times\boldsymbol{a}_6)^T & -{}^0R_1\boldsymbol{a}_6^T & (C_6\times\boldsymbol{a}_6)^T \end{bmatrix},$$

$$A_i={}^0R_1\,{}^1\mathbf{p}_i,$$

$$B_i={}^0R_1\,{}^1\mathbf{t}-{}^0R_1\,{}^1R_2\,{}^2R_0\boldsymbol{b}_i+{}^2R_0\boldsymbol{b}_i+{}^0R_1\,{}^1R_2\,{}^2\boldsymbol{p}_i,$$

$$C_i={}^1R_2\,{}^2R_0\boldsymbol{b}_i-{}^2R_0\boldsymbol{b}_i-{}^1R_2\,{}^2\boldsymbol{p}_i, \quad i=1,2,\ldots,6.$$

Now, moving M to the other side yields

$$\dot{\mathbf{o}}=M^{-1}L\dot{\mathbf{l}}=J_v\dot{\mathbf{l}}, \tag{24}$$

where $J_v=M^{-1}L$ is called the velocity Jacobian matrix of the paramill.

4.2. Force/Moment Jacobian Matrix

The force/moment Jacobian matrix relates the forces acting at the 12 legs with the force/moment resulting on the platforms. Therefore, the rolling force and moment needed at the work-rolls can be generated by multiplying the force/moment Jacobian matrix at a given configuration to the force vector of 12 legs. Now, this relationship is derived from the principle of virtual work as follows:

Taking the variations of both sides of (24) yields

$$\delta\mathbf{o}=J_v\delta\mathbf{l}, \tag{25}$$

where $\delta\mathbf{o}=[\delta d_X \ \delta d_Y \ \delta d_Z \ \delta\alpha \ \delta\beta \ \delta\gamma \ \delta t_x \ \delta t_y \ \delta t_z \ \delta\alpha_{pc} \ \delta\beta_{pc} \ \delta\gamma_{pc}]^T$ and $\delta\mathbf{l}=[\delta\|a_1\|\cdots\delta\|a_6\|\delta\|a_1\|\cdots\delta\|a_6\|]^T$. Let $\mathbf{f}\triangleq[f_{l1}\cdots f_{l6} \ f_{u1}\cdots f_{u6}]^T$ be the actuating forces at the legs. Let $F=[F_X \ F_Y \ F_Z \ F_{rollx} \ F_{rolly} \ F_{rollz}]^T$ and $M=[M_X \ M_Y \ M_Z \ M_{pcx} \ M_{pcy} \ M_{pcz}]^T$ be the rolling force and moment at the lower work-roll, respectively.

The application of the principle of virtual work to (25) yields

$$\mathbf{f}^T\delta\mathbf{l}=\boldsymbol{\tau}^T\delta\mathbf{o}. \tag{26}$$

The substitution of (25) into (26) yields:

$$(\mathbf{f}^T-\boldsymbol{\tau}^TJ_v)\delta\mathbf{l}=0. \tag{27}$$

Since $(\delta\mathbf{l})$ in (27) is linearly independent,

$$\mathbf{f}=J_v^T\boldsymbol{\tau}. \tag{28}$$

Defining $J_f\triangleq(J_v^T)^{-1}$, (28) becomes

$$\boldsymbol{\tau}=J_f\mathbf{f}, \tag{29}$$

where J_f is termed the force/moment Jacobian matrix, which maps the actuating forces at the legs to the resultant force and moment at the end-effector. Since J_v in (24) and J_f in (29) relate the input magnitudes with the output velocities and force/moment, they can be used as a tool for analyzing the manipulability of the structure.

4.3. The Workspace

It may suffice to define a workspace for the lower SP because that for the upper one can be defined in a similar way. Using the definition of the workspace introduced in Reference 3, the following two workspaces are defined.

First, focusing on translational motions, the position workspace, which represents the extent that the center point of the work-roll can reach to, is defined as follows:

$$\Omega=\{(\Delta X,\Delta Y,\Delta Z)|-70\leqslant\Delta X\leqslant 70,$$
$$-100\leqslant\Delta Y\leqslant 100, \quad 0\leqslant\Delta Z\leqslant 150;$$
$$\text{unit}=\text{mm}\}, \tag{30}$$

where ΔX, ΔY, and ΔZ are incremental displacements of the work-roll in the X-Y-Z directions from

Table I. Workspace specifications.

6 DOF motions		Lower SP	Upper SP	Control objectives
Translational motions	Strip moving direction (surge)	±70 mm	±70 mm	Tension control
	Roll sideward shift (sway)	±100 mm	±100 mm	Uniform roll wear
	Strip thickness direction (heave)	150 mm	150 mm	Thickness control
Rotational motions	Rotation about the X-axis (roll)	±1.42°	±1.42°	Even wear
	Rotation about the Y-axis (pitch)	N/A	N/A	N/A
	Rotation about the Z-axis (yaw)	±1°	±1°	Uniform strip thickness

the static neutral configuration. Also, at the given neutral position of the roll, the orientation workspace, which represents how far the roll can rotate, is defined as follows:

$$\Delta = \{(\alpha, \beta, \gamma) | -1.42 \leqslant \alpha \leqslant 1.42, \beta = 0, -1 \leqslant \gamma \leqslant 1; \text{unit} = ^\circ\}, \tag{31}$$

where α, β, and γ are the rotational angles of the work-roll in fixed angle representation. Note that there is no pitch motion in the orientation workspace. The 6 DOF motions of the roll, specifications, and their control objectives are summarized in Table I.

Because the extent of the orientation workspace in the rolling process is very small and its consequence is somewhat limited due to the smallness, only the position workspace is considered in the manipulability analysis in the next section. However, the orientation workspace can be utilized in a later stage when determining the maximum/minimum lengths of hydraulic cylinders. Finally, it is noted that a kinematic singularity does not exist within the workspace given by (30) and (31).

5. KINEMATIC OPTIMAL DESIGN

5.1. Manipulability Analysis

One might want to know how easily the mechanism can be manipulated in terms of delivering velocities and forces.[14–18] That is, it would be desirable to achieve the target jobs in the configuration space with minimal efforts in the joint space.

To analyze input–output characteristics of a given mechanism, a unit-norm input is often used. But, the unit-norm input may not represent the actual operating range of the mechanism because the maximum velocities and forces of individual actuators may differ. Therefore, individual actuator velocity and force must be normalized.[19,20] Now, the normalized input velocities and forces are defined as follows:

$$\hat{\dot{\mathbf{l}}} \triangleq W_l^{-1} \dot{\mathbf{l}}, \tag{32}$$

$$\hat{\mathbf{f}} \triangleq W_f^{-1} \mathbf{f}, \tag{33}$$

where $W_l = \text{diag}(\|\dot{\mathbf{a}}_1\|_{\max} \cdots \|\dot{\mathbf{a}}_6\|_{\max} \|\dot{a}_1\|_{\max} \cdots \|\dot{a}_6\|_{\max})$ and $W_f = \text{diag}(f_{l1\,\max} \cdots f_{l6\,\max} f_{u1\,\max} \cdots f_{u6\,\max})$ represent the maximum velocities and forces generated on the twelve actuators and ˆ denotes the normalized value. Here, noting that the arrangement of the 12 hydraulic cylinders is symmetrical, we can assume that the maximum velocities and forces of all actuators are equal. Thus, in the case of a paramill, W_l and W_f can be assumed diagonal matrices with proper weightings.

The substitution of (32) and (33) into (24) and (29), respectively, yields

$$\begin{bmatrix} \mathbf{v}_l \\ \boldsymbol{\omega}_l \\ \mathbf{v}_{roll} \\ \boldsymbol{\omega}_{pc} \end{bmatrix} = (J_v^{-1} W_l)\dot{\hat{\mathbf{l}}}, \tag{34}$$

$$\begin{bmatrix} \mathbf{F}_l \\ \mathbf{M}_l \\ \mathbf{F}_{roll} \\ \mathbf{M}_{pc} \end{bmatrix} = (J_f W_f)\hat{\mathbf{f}}, \tag{35}$$

where $\mathbf{v}_l$, $\boldsymbol{\omega}_l$, $\mathbf{F}_l$, and $\mathbf{M}_l$ denote the velocity, angular velocity, force, and moment of the lower work-roll; $\mathbf{v}_{roll}$, $\boldsymbol{\omega}_{pc}$, $\mathbf{F}_{roll}$, and $\mathbf{M}_{pc}$ represent the relative velocity, relative angular velocity, rolling force, and rolling moment between the two work-rolls.

It is noted that the variables related to the lower SP, i.e., $\mathbf{v}_l$, $\boldsymbol{\omega}_l$, $\mathbf{F}_l$, $\mathbf{M}_l \in \mathbf{R}^{3\times 1}$, have been included for computational purpose. In (34) and (35), the variables that deserve attention are $\mathbf{v}_{roll}$, $\boldsymbol{\omega}_{pc}$, $\mathbf{F}_{roll}$ and $\mathbf{M}_{pc}$, which are the roll gap velocity, angular velocity of the pair-crossing, rolling force, and rolling moment.

Now, splitting the Jacobian matrices of (34) and (35) into two parts, the relative motion (linear and angular) of two work-rolls and rolling force/moment are finally derived as follows:

$$\begin{bmatrix} \mathbf{v}_{roll} \\ \boldsymbol{\omega}_{pc} \end{bmatrix} = \begin{bmatrix} \hat{J}_{\mathbf{v}o} \\ \hat{J}_{\boldsymbol{\omega}o} \end{bmatrix} \dot{\hat{\mathbf{l}}}, \tag{36}$$

$$\begin{bmatrix} \mathbf{F}_{roll} \\ \mathbf{M}_{pc} \end{bmatrix} = \begin{bmatrix} \hat{J}_{\mathbf{F}o} \\ \hat{J}_{\mathbf{M}o} \end{bmatrix} \hat{\mathbf{f}}, \tag{37}$$

where $\mathbf{v}_{roll}$, $\boldsymbol{\omega}_{pc}$, $\mathbf{F}_{roll}$, $\mathbf{M}_{pc} \in \mathbf{R}^{3\times 1}$, $\hat{J}_{\mathbf{v}o}$, $\hat{J}_{\boldsymbol{\omega}o}$, $\hat{J}_{\mathbf{F}o}$, $\hat{J}_{\mathbf{M}o} \in \mathbf{R}^{3\times 12}$, and the subscript o denotes "output." Since all analyses of the four split Jacobian matrices in (36) and (37) are the same, we carry out only one analysis as a representative one.

Intuitively, the manipulability can be defined as how easily and uniformly the end-effector is able to move in an arbitrary direction. To analyze the manipulability of a mechanism, the manipulability ellipsoid is the most intuitive and useful measure. It can be made by mapping a unit sphere in the input space to the output space through the Jacobian matrix. The major and minor axes of the ellipsoid indicate the directions in which the platform can move most and least easily, respectively, and the ease is proportional to the principal axis length. Also, the magnitude and direction of the major and minor axes can be obtained from the singular value decomposition. If the ellipsoid is larger and more circular, then the platform has faster velocity, larger forces, and more uniform motion. The volume of the output manipulability ellipsoid (MEV) and the condition number (CN) for a given weighted Jacobian matrix are defined as follows:[12]

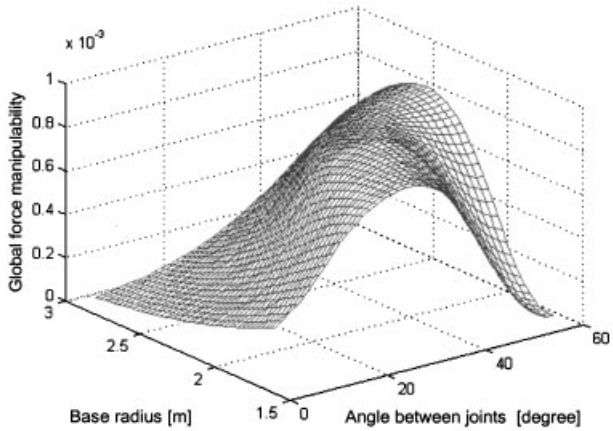

(a) 3D plots of the global force manipulability measure.

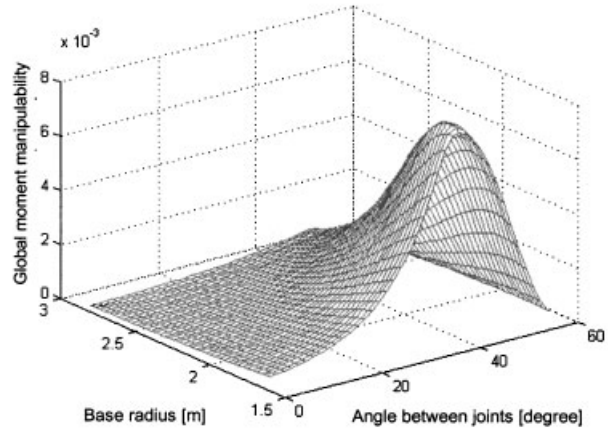

(b) 3D plots of the global moment manipulability measure.

Figure 6. Three-dimensional plots of the global force and moment manipulability measures with the use of one SP (Ref. 3).

$$\mathrm{MEV} \triangleq \frac{\pi^{\nu/2}}{\Gamma(1+\nu/2)} \prod_{i=1}^{\nu} \sigma_i, \tag{38}$$

$$\mathrm{CN} \triangleq \frac{\sigma_{\max}}{\sigma_{\min}}, \tag{39}$$

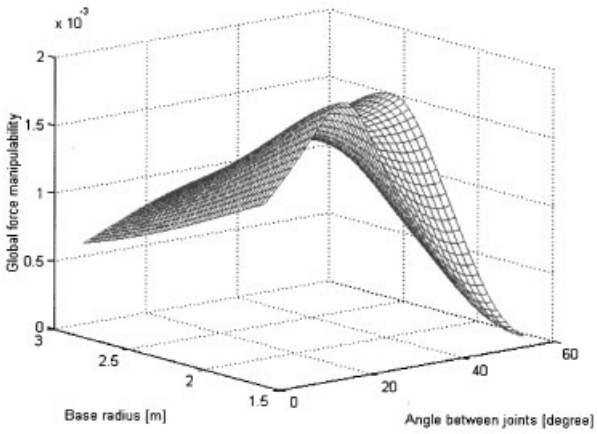

(a) 3D plots of the global force manipulability measure.

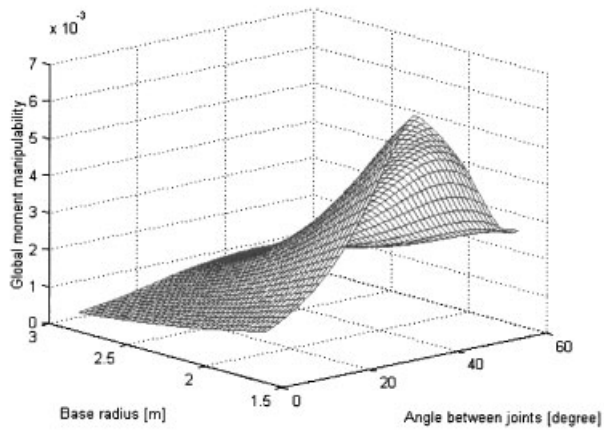

(b) 3D plots of the global moment manipulability measure.

Figure 7. Three-dimensional plots of the global force and moment manipulability measures with the use of two SPs.

where ν is the dimension of the manipulability ellipsoid and $\Gamma(\cdot)$ is the gamma function. The condition number represents the directional characteristics of the Jacobian matrix. The larger the condition number is, the more severe the directional characteristics is. The larger the volume of the manipulability ellipsoid is, the greater the total output is for a given input. Therefore, it is desirable to have a small condition number and a large volume. Therefore, both MEV and CN must be combined for a kinematic optimal design.

Integrating local manipulabilities over the given workspace, the following global manipulability index can be defined:

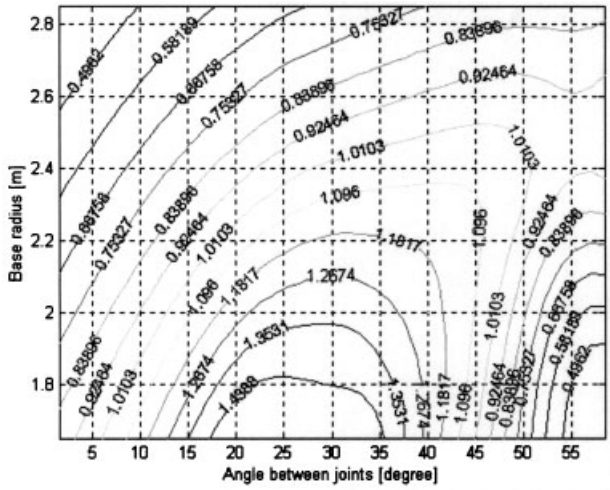

Figure 8. Two-dimensional contours of the combined global force and moment manipulability measures with the use of two SPs.

$$\Lambda_i = \frac{\int_\Omega \lambda_i(r_{lb}, r_{ub}, \phi_{lb}, \phi_{ub}, \phi_{lp}, \phi_{up}) d\Omega}{\int_\Omega d\Omega}, \quad i = 1,2,3,4, \tag{40}$$

where Ω, λ_i, and Λ_i represent the total workspace, the local manipulability measure, and the global manipulability, respectively.

Finally, it is noted that these manipulabilities are functions of the kinematic parameters concerned. If the velocity manipulability is large, then the mechanism can respond fast and, furthermore, the response characteristics are uniform throughout the workspace. Similarly, if the force/moment manipulability is large, the mechanism can resist a large external disturbance and its resistance characteristics are isotropic.

In order to confirm the correctness of the proposed method, the results of the proposed method and the results in Reference 3 are compared. Figure 6 shows the 3-D plots of the global force and moment manipulability measures obtained with the use of one SP (see Reference 3). Figure 7 shows the 3-D plots of the global force and moment manipulability measures obtained with the use of two SPs. It can be seen from Figures 6(a) and 7(a) that the maximum value of the global force manipulability in Figure 7(a) is greater than that of Figure 6(a). The reason for this is that the condition number is the same, but the manipulability ellipsoid volume for the case of two SPs is bigger than the case of one SP. That is, with the same parameter values and the same input forces, the maximum output in the case of two SPs is larger than

Table II. The ranges of maximizing kinematic parameters.

	$r_{lb}=r_{ub}$ (mm)	$2\phi_{lp}=2\phi_{up}$ (°)	$2\phi_{lb}=2\phi_{ub}$ (°)	Remark
Global force manipulability	1620–1820	17.5–35.5	17.5–35.5	Important
Global moment manipulability	1620–1820	17.5–35.5	17.5–35.5	Important
Global translational velocity manipulability	1850, 2850	60	60	Less important
Global rotational velocity manipulability	2850	60	60	Less important

that of a single SP, which means that for given magnitudes of desired rolling force/moment, the actuator sizes can be compactly designed. This is very important because this will allow the reduction of a stand size and consequently the length of the entire production line. On the other hand, from Figures 6(b) and 7(b) it can be seen that the moment manipulabilities are almost the same. The reason for this can be traced from the fact that the rotational workspace for the rolling process is relatively small compared with the translational workspace.

5.2. Determination of Kinematic Parameters

Let a static neutral position of the work-roll be $\mathbf{d}=-\boldsymbol{d}=[0\ \ 0\ \ 0.8]^T$ with ${}^1R_2={}^0R_1={}^0R_2=\mathrm{I}$, where I is an identity matrix. The position and orientation of the work-roll can be expressed as deviations from the static neutral position.

The ranges of parameter values in the pursuit of optimal design are set as follows:

$$0°<2\phi<60°,$$

$$1620\ \ \mathrm{mm}\leqslant r\leqslant 2852\ \ \mathrm{mm},$$

where $\phi=\phi_{lb}=\phi_{lp}=\phi_{ub}=\phi_{up}$ and $r=r_{lb}=r_{ub}$ have been assumed. The defined ranges have the following interpretations: The 0° angle between two joints means that the joints of two neighboring cylinders are overlapped at one point. This means that the SP will allow less DOF motions. And the 60° of acute angle results in a singular configuration.[6,7] The base radius of $r_{lb}=r_{ub}\geqslant 1620$ mm represents that the base diameter must be larger than the length of a work-roll. The range $r_{lb}=r_{ub}\leqslant 2850$ mm is limited from the size of a stand. Because all above values were taken for demonstration purpose, they can be changed in a later stage reflecting the actual conditions. If the base and platform radii become identical, the moment manipulability becomes maximized.

Figure 8 shows the two-dimensional contours of the combined global force and moment manipulabilities in Figure 7. The reason for adding two manipulabilities is because it is difficult to figure out the maximum parameter values that satisfy both the force and moment manipulabilies at the same time. Note that the two manipulabilities have different units. Therefore, both manipulabilities were first normalized by their peak values and then added.

It is finally observed that a common range that maximizes both manipulabilities is 1620–1820 mm for the case of radius and 17.5°–35.5° for the case of joint angle. Assuming that the paramill operates in the workspace defined in Section 4.3, $\mathbf{a}_i$ $(i=1,2,...,6)$ can be obtained from (1) and therefore the minimum and maximum lengths of the actuators can be calculated from (10) because $\mathbf{b}_i$, $\mathbf{p}_i$, $\boldsymbol{b}_i$, $\boldsymbol{p}_i$, $i=1,2,...,6$, are

Table III. Final specifications obtained by kinematic optimization: single SP case.

	Platform radius (r_p)	Base radius (r_b)	Angle between joints ($\phi_b=\phi_p$)	Minimum length of leg ($l_{\min}$)	Maximum length of leg ($l_{\max}$)
Kinematic optimization	1620 mm	1900 mm	41°	907.7 mm	1269.3 mm

Table IV. Final specifications obtained by kinematic optimization: two SPs case.

	Platform radius ($r_{lp}=r_{up}$)	Base radius ($r_{lb}=r_{ub}$)	Angle between joints ($2\phi_{lb}=2\phi_{lp}$) ($2\phi_{ub}=2\phi_{up}$)	Minimum length of leg ($l_{\min}$)	Maximum length of leg ($l_{\max}$)
Kinematic optimization	1620 mm	1800 mm	32°	716.6 mm	1730.3 mm

determined from the kinematic design; ${}^0R_1$ and ${}^2R_0$ are determined by the given workspace; and ${}^1R_2$ is determined by ${}^0R_1$ and ${}^0R_2$. And, **t** will be determined from the positional workspace.

Now, the kinematic parameters that maximize the global force and moment manipulabilities are gathered in Table II. For rolling, the transmissions of force and moment are more important than those of velocity and angular velocity. This is because maintaining the rolling force and moment is more critical than a fast change of the roll gap and the pair-crossing angle. Table III shows the optimal results obtained with the use of single SP in Reference 3, while the results with the use of two SPs are gathered in Table IV. By comparing Tables III and IV, it is seen that the base can be made smaller through the analysis of two SPs, which will allow the smaller size of a stand, and again which makes the entire production line shorter.

6. CONCLUSIONS

In this paper a feasibility study on a new parallel-type rolling mill based upon two SPs was investigated. Because an advantage of using different base sizes in the lower and upper SPs was not seen, both SPs were assumed to have the same structure, but used in opposite directions. The forward kinematics problem was finding the roll-gap and the pair-crossing angle of the two work-rolls for given lengths of the 12 legs. On the other hand, the inverse kinematics problem was finding the lengths of 12 legs when the roll-gap, the pair-crossing angle, and the position and orientation of one work-roll were given. Two important kinematic parameters, the size of the base and the acute angle made by two neighboring joints for a given size of the work-roll, have been determined in such a way that the force and moment transmissions from the actuators to the work-roll is maximized. It is the authors' desire that the results in this paper provide a guideline for the conceptual design of parallel-type rolling mills of SP type. Future works would be a dynamics analysis and an integrated control of the strip thickness, strip tension, roll speed, strip shape, pair-crossing angle, uniform wear of the roll, etc.

ACKNOWLEDGMENT

This work was supported by the Ministry of Science and Technology of Korea under a program of the National Research Laboratory, Grant No. NRL M1-0302-00-0039-03-J00-00-023-10.

REFERENCES

1. E.F. Fichter, A SP based manipulator: General theory and practical construction, Int J Robot Res 5:(2) (1986), 157–181.
2. J.P. Merlet, Parallel robots, Kluwer Academic, Dordrecht, 2000, pp. 91–91.
3. K.S. Hong, K.T. Hong, C. Choi, and W.S. Yoo, Kinematic optimal design of a new parallel-type rolling mill: paramill, Adv Rob 17 (9) (2003), 837–862.
4. E.M. Mielnik, Metalworking science and engineering, McGraw-Hill, New York, 1991.
5. Y. Bissessur, E.B. Martin, A.J. Morris, and P. Kitson, Fault detection in hot steel rolling using neural networks and multivariate statistics, IEE Proc Control Theory Applic 147:(6) (2000), 633–640.
6. C.M. Gosselin and J. Angeles, Singularity analysis of closed-loop kinematic chains, IEEE Trans Robot Autom 6:(3) (1990), 281–290.
7. O. Ma and J. Angeles, Architecture singularities of platform manipulators, Proc IEEE Int Conf on Robotics and Automation, Sacramento, CA, 1991, pp. 1542–1547.
8. F.C. Park and J.W. Kim, Singularity analysis of closed kinematic chains, ASME Trans J Mech Des 121:(1) (1999), 32–38.
9. M.K. Lee and K.W. Park, Workspace and singularity analysis of a double parallel manipulator, IEEE/ASME Trans Mechatron 5:(4) (2000), 367–375.
10. L. Baron and J. Angeles, The direct kinematics of parallel manipulators under joint-sensor redundancy, IEEE Trans Robot Autom 16:(1) (2000), 12–19.
11. P. Nanua, K.J. Waldron, and V. Murthy, Direct kinematic solution of a Stewart platform, IEEE Trans Robot Autom 6:(4) (1990), 438–444.
12. B.J. Ahn and K.S. Hong, Force/moment transmission-

ability analysis of a parallel manipulator, J Korean Soc Precision Eng 13:(4) (1996), 109–121.
13. M.W. Spong and M. Vidyasagar, Robot dynamics and control, Wiley, New York, 1989, pp. 55–56.
14. T. Yoshikawa, Manipulability of robotic mechanisms, Int J Robot Res 4:(2) (1985), 3–9.
15. M. Uchiyama, Structures and characteristics of parallel manipulators, Adv Robot 8:(6) (1994), 545–557.
16. K.E. Zanganeh and J. Angeles, Kinematic isotropy and the optimum design of parallel manipulators, Int J Robot Res 16:(2) (1997), 185–197.
17. F.C. Park and J.W. Kim, Manipulability of closed kinematic chains, ASME Trans J Mech Des 120:(4) (1998), 542–548.
18. H. Yoshida, K. Inoue, T. Arai, and Y. Mae, Mobile manipulation of humanoid robots, Proceedings IEEE/ASME Int Conf on Advanced Intelligent Mechatronics, Como, Italy, 8–12 July 2001, pp. 266–271.
19. K.S. Hong and J.G. Kim, Manipulability analysis of a parallel machine tool: Application to optimal link parameter design, J Robot Syst 17:(8) (2000), 403–415.
20. M. Araki and H. Taguchi, Two-degree-of-freedom PID controllers, Int J Control, Automation, Syst 1:(4) (2003), 401–411.